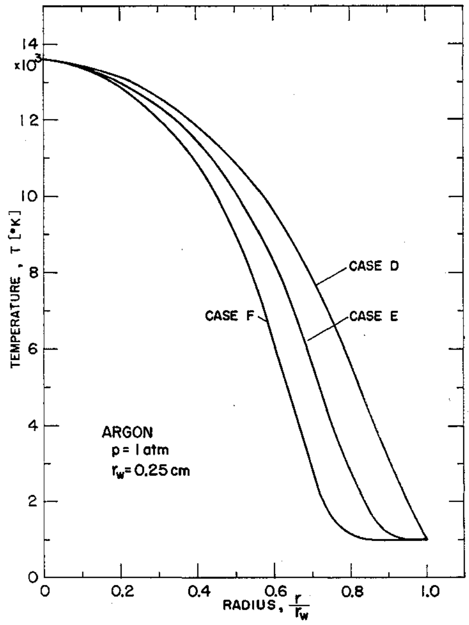

Fig. 4 Influence of uncertainties of the volumetric radiation on the temperature profiles of a transpiration-cooled arc.

P_r from Ref. 9. Case C: ρ, c_p, h from Ref. 10; k, σ, P_r from Ref. 7; μ from Ref. 6.

For the low-temperature range ($T < 3{,}000°K$), the gas properties from Ref. 11 have been used. Since the peak temperature is relatively low, the influence of the volumetric radiation is almost negligible in this range. In addition, the values of the electrical conductivity used for the calculations are in much better agreement from author to author than those of the thermal conductivity. Therefore, the spread of the different calculated temperature profiles is caused mainly by uncertainties of the thermal conductivities. The effect of this uncertainty on the arc characteristics is demonstrated in Table 1, which contains calculated values of the electric field strength, the electric current, the power input, the mass injection rate through the porous wall, and the mass average enthalpy for cases A, B, and C.

The influence of the not-well-known volumetric radiation on the arc characteristics and the temperature profiles is evident from Fig. 4 and Table 2. The calculations are based on the following gas properties. Case D: ρ, c_p, h from Ref. 10; k, σ, μ from Ref. 6; $P_r = 0$. Case E: ρ, c_p, h from Ref. 10; k, σ, μ from Ref. 6; P_r from Ref. 9. Case F: ρ, c_p, h from Ref. 10; k, σ, μ from Ref. 6; P_r from Ref. 7.

In this case the peak temperature reached the value of 13,600°K and the temperature at the wall was 1,000°K. Neglecting the volumetric radiation entirely or using the values given in Ref. 7 leads to deviations in the temperature profiles of up to 5000°K. The disagreement of the arc characteristics is shown in Table 2.

From these examples which have been taken from a large number of calculations, it is obvious that the uncertainties in the plasma transport properties cause large uncertainties of the temperature distributions and arc characteristics of a transpiration-cooled arc. Because of this problem, a quantitative comparison of analytical and experimental results is presently nearly impossible. Comparisons can be undertaken only to demonstrate agreement of basic trends.

Table 1 Influence of the thermal conductivity on arc characteristics

Case	E, v/cm	I, amp	EI, kw/cm	$\dot{m}$, g/cm^2 sec	H, kjoules/kg
A	4.25	36.5	0.155	0.01841	2687
B	5.37	53.0	0.285	0.02669	3400
C	5.39	59.8	0.322	0.02854	3595

Table 2 Influence of the volumetric radiation on arc characteristics

Case	E, v/cm	I, amp	EI, kw/cm	$\dot{m}$, g/cm^2 sec	H, kjoules/kg
D	10.64	42.6	0.453	0.0531	5431
E	13.12	41.2	0.54	0.0821	3835
F	15.13	37.3	0.57	0.1009	3231

References

[1] Pfender, E., Gruber, G., and Eckert, E. R. G., "Experimental Investigations of a Transpiration-Cooled, Constricted Arc," *Proceedings of the VIIIth International Conference on Phenomena of Ionized Gases*, Springer-Verlag, Berlin, Germany, 1967, p. 230.

[2] Pfender, E., Gruber, G., and Eckert, E. R. G., "Experimental Investigation of a Transpiration-Cooled, Constricted Arc," *Proceedings of the IIIrd International Symposium on High Temperature Technology*, Butterworths, London, to be published.

[3] Anderson, J. E., "Transpiration Cooling of a Constricted Electric-Arc Heater," Rept. ARL 66-0157, 1966, Aerospace Research Labs.

[4] Anderson, J. E. and Eckert, E. R. G., "Performance Characteristics of a Fully-Developed Constricted Transpiration-Cooled Arc," *AGARDograph 84*, Pt. II, p. 751.

[5] Anderson, J. E. and Eckert, E. R. G., "Transpiration Cooling of a Constricted Electric-Arc Heater," *AIAA Journal*, Vol. 5, No. 4, April 1967, pp. 699–706.

[6] Devoto, R. S., "Transport Coefficient of Partially Ionized Argon," *The Physics of Fluids*, Vol. 10, No. 2, Feb. 1967, pp. 354–363.

[7] Emmons, H. W., "The Arc Measurements of High Temperature Gas Transport Properties," *The Physics of Fluids*, Vol. 10, No. 6, June 1967, pp. 1125–1136.

[8] Knopp, E. F., "An Experimental Determination of the Thermal and Electrical Conductivity of Atmospheric Argon Plasma," NU-GDL Report B-1-65, 1965, Northwestern Univ.

[9] Olsen, H. N., "Partition Function Cutoff and Lowering of the Ionization Potential in an Argon Plasma," *The Physical Review*, Vol. 124, No. 6, Dec. 1961, p. 703.

[10] Drellishak, K. S., Knopp, C. T., and Cambel, A. B., "Partition Functions and Thermodynamic Properties of Argon Plasma," NU-GDL Report A-3-62, 1962, Northwestern Univ.

[11] Hilsenrath, J., *Tables of Thermodynamic and Transport Properties of Air, Argon, Carbon Dioxide, Hydrogen, Nitrogen, Oxygen and Steam*, Pergamon, New York, 1960.

[12] Penski, K., "Zustands- und Transportgrössen von Argon-Plasma," *Chemie Ingenieur-Technik*, Vol. 34, 1962, p. 84.

Light Antiaircraft Projectile Ballistics

JOHN W. MILENSKI JR.*
Braddock, Dunn and McDonald Inc., El Paso, Texas

Nomenclature

$\bar{A}$ = reference area for drag coefficient
C_D = drag coefficient
$\bar{D}$ = $C_D \frac{1}{2}\bar{\rho}\bar{v}^2\bar{A}$ = aerodynamic drag force
$\bar{g}$ = acceleration of gravity
$\bar{m}$ = projectile mass
$\bar{S}_D$ = $2\bar{m}/C_D\bar{\rho}\bar{A}$ = aerodynamic penetration
$\bar{t}$ = time
$\bar{v}$ = projectile velocity
$\bar{y}$ = horizontal (downrange) coordinate
$\bar{z}$ = vertical (altitude) coordinate

Received November 25, 1968; revision received July 9, 1969.
* Senior Analyst, Flight Mechanics Group. Member AIAA.

γ = flight-path angle
ϵ = $2\bar{m}\bar{g}/C_D\bar{\rho}\bar{v}_m{}^2\bar{A}$ = projectile weight to initial drag force ratio
$\bar{\rho}$ = atmospheric air density
$\bar{\tau}$ = $\bar{S}_D/\bar{v}_m$ = projectile time constant

Subscript

$(\ )_m$ = initial condition at gun muzzle

Introduction

PROJECTILE ballistics occupy an important role when evaluating the effectiveness of light caliber antiaircraft guns employed against high-speed, low-altitude targets. In particular, projectile attitude angle and gravity drop require special attention. Attitude angle is important because it must be known to determine the angle of obliquity at target impact. Gravity drop is of concern because it is required (together with other considerations) by many fire control systems in order to generate superelevation angle.

Certain aspects of ballistics have recently been discussed by Larrabee[1] and Smith.[2] Projectile deceleration was treated by Larrabee, but no attempt was made to determine analytical time solutions for projectile attitude angle and gravity drop. Smith presented an approximate solution for wind drift and discussed gravity drop, although in limited detail.

Earlier work dealing with approximate methods applicable to light antiaircraft projectile ballistics is presented by McShane, Kelley, and Reno.[3] Included among these methods is one widely employed by ballisticians and originally devised by Popoff.

The present Note represents a considerable extension of the work by Larrabee and Smith in that it provides approximate time solutions to projectile velocity, attitude angle, gravity drop, and downrange. Solutions are obtained and expressed in such a manner that comparisons can readily be made with those presented elsewhere.

Analysis

For well-designed spin stabilized projectiles, the trajectory may be taken to lie in the plane of departure and the attitude and flight-path angles may be treated interchangeably. Air density can be considered essentially constant since the altitudes of interest are less than a few hundred meters above the gun muzzle.

From the geometry shown in Fig. 1, projectile velocity and flight-path (attitude) equations of motion are:

$$\bar{m}(d\bar{v}/d\bar{t}) = -\bar{m}\bar{g}\sin\gamma - C_D\tfrac{1}{2}\bar{\rho}\bar{v}^2\bar{A} \tag{1a}$$

$$\bar{m}\bar{v}(d\gamma/d\bar{t}) = -\bar{m}\bar{g}\cos\gamma \tag{1b}$$

The downrange and altitude kinematic equations are

$$d\bar{y}/d\bar{t} = \bar{v}\cos\gamma \tag{2a}$$

$$d\bar{z}/d\bar{t} = \bar{v}\sin\gamma \tag{2b}$$

It is convenient to rewrite (1) and (2) in dimensionless form. This can be achieved by first defining the following

Table 1 Trajectory variables, $\gamma_m = 1.5°$

	Exact solution				Approximate solution			
$\bar{t}$, sec	$\bar{v}$, m/sec	γ, deg	$\bar{y}$,m	$\bar{z}$,m	$\bar{v}$, m/sec	γ, deg	$\bar{y}$,m	$\bar{z}$,m
0.0	1050.0	1.50	0.0	0.0	1050.0	1.50	0.0	0.0
0.5	847.8	1.20	470.7	11.2	847.8	1.20	470.7	11.2
1.0	710.9	0.84	858.3	18.1	710.9	0.84	858.3	18.1
1.5	612.1	0.41	1187.9	21.8	612.0	0.41	1187.9	21.8
2.0	537.4	−0.08	1474.4	22.7	537.3	−0.08	1474.4	22.7
2.5	479.0	−0.64	1728.0	21.1	478.8	−0.63	1728.0	21.1
3.0	432.1	−1.25	1955.3	17.4	431.7	−1.25	1955.4	17.4
3.5	393.7	−1.93	2161.4	11.7	393.1	−1.93	2161.5	11.7
4.0	361.6	−2.68	2349.8	4.2	360.8	−2.68	2350.0	4.2
4.5	334.4	−3.49	2523.4	−5.1	333.3	−3.49	2523.7	−5.1

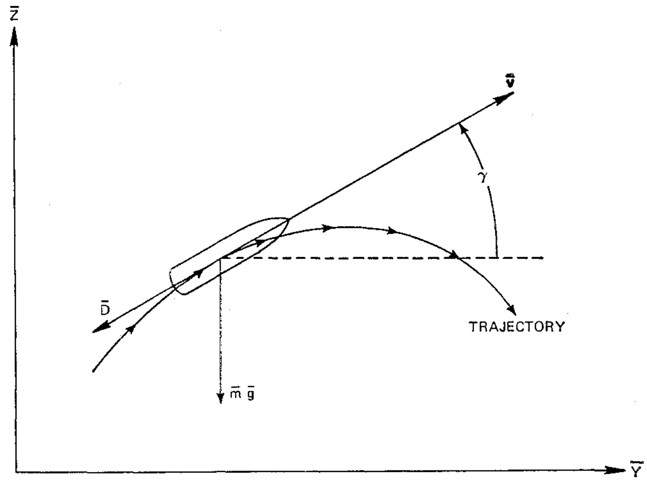

Fig. 1 Trajectory geometry.

nondimensional variables:

$$v = \bar{v}/\bar{v}_m,\ y = \bar{y}/\bar{S}_D,\ z = \bar{z}/\bar{S}_D,\ t = \bar{t}/\bar{\tau}$$

where

$$\bar{S}_D = 2\bar{m}/C_D\bar{\rho}\bar{A},\ \bar{\tau} = \bar{S}_D/\bar{v}_m$$

$\bar{v}_m$ is the projectile velocity at the gun muzzle, $\bar{S}_D$ is Larrabee's aerodynamic penetration[1] and $\bar{\tau}$ is the defined projectile time constant.

Introducing these dimensionless variables into (1) and (2) and employing the sine of the flight-path angle as a dependent variable yield

$$dv/dt = -\epsilon\sin\gamma - v^2 \tag{3a}$$

$$v(d\sin\gamma/dt) = \epsilon(\sin^2\gamma - 1) \tag{3b}$$

$$dy/dt = v(1 - \sin^2\gamma)^{1/2} \tag{4a}$$

$$dz/dt = v\sin\gamma \tag{4b}$$

The dimensionless parameter ϵ appearing in (3) is the ratio of projectile weight to initial drag force where the drag force is based on an equivalent constant or average drag coefficient. For modern high-speed, low-drag light antiaircraft projectiles, ϵ is on the order of 2 or 3%. The presence of the small parameter ϵ suggests that the dependent variables be expanded as series in powers of ϵ, e.g.,

$$v(t,\epsilon) = v_0(t) + \epsilon v_1(t) + 0(\epsilon^2) \text{ etc.} \tag{5}$$

Substituting series for v and $\sin\gamma$ into (3), equating like coefficients of the parameter ϵ, integrating the resultant recursive equations, and taking into account the initial muzzle conditions yield

$$v = \frac{1}{(1+t)} + \epsilon\left(\frac{\sin\gamma_m}{3}\right)\left[\frac{1}{(1+t)^2} - (1+t)\right] + 0(\epsilon^2) \tag{6a}$$

$$\sin\gamma = \sin\gamma_m + \epsilon\left(\frac{\cos^2\gamma_m}{2}\right)[1 - (1+t)^2] + 0(\epsilon^2) \tag{6b}$$

Substituting series for y and z together with (6) into (4) allows solutions for the downrange and altitude variables to be found in a similar manner, although a slight increase in algebraic manipulation is involved. These solutions

Table 2 Trajectory variables, $\gamma_m = 10.0°$

	Exact solution				Approximate solution			
$\bar{t}$, sec	$\bar{v}$, m/sec	γ, deg	$\bar{y}$,m	$\bar{z}$,m	$\bar{v}$, m/sec	γ, deg	$\bar{y}$,m	$\bar{z}$,m
0.0	1050.0	10.00	0.0	0.0	1050.0	10.00	0.0	0.0
0.5	847.2	9.70	463.7	80.6	847.2	9.70	463.7	80.6
1.0	709.9	9.35	845.7	144.8	709.9	9.35	845.7	144.8
1.5	610.7	8.92	1170.4	197.1	610.6	8.93	1170.5	197.1
2.0	535.7	8.44	1452.9	240.3	535.6	8.45	1452.9	240.3
2.5	477.0	7.89	1703.0	276.2	476.7	7.90	1703.0	276.2
3.0	429.8	7.27	1927.3	306.0	429.4	7.30	1927.4	306.1
3.5	391.1	6.59	2130.7	330.8	390.5	6.63	2130.9	330.9
4.0	358.7	5.84	2316.8	351.1	357.9	5.90	2317.0	351.2
4.5	331.3	5.03	2488.4	367.5	330.3	5.12	2488.7	367.6

Table 3 Trajectory variables, $\gamma_m = 20.0°$

	Exact solution				Approximate solution			
$\bar{t}$, sec	$\bar{v}$, m/sec	γ, deg	$\bar{y}$,m	$\bar{z}$,m	$\bar{v}$, m/sec	γ, deg	$\bar{y}$,m	$\bar{z}$,m
0.0	1050.0	20.00	0.0	0.0	1050.0	20.00	0.0	0.0
0.5	846.6	19.72	442.5	159.9	846.6	19.72	442.5	159.9
1.0	708.7	19.37	807.0	289.4	708.7	19.37	807.0	289.4
1.5	609.1	18.97	1117.0	397.2	609.0	18.98	1117.0	397.2
2.0	533.8	18.50	1386.8	488.8	533.6	18.52	1386.8	488.8
2.5	474.7	17.97	1625.7	567.6	474.5	18.01	1625.7	567.6
3.0	427.2	17.38	1840.1	635.9	426.8	17.43	1840.2	636.0
3.5	388.1	16.72	2034.7	695.6	387.6	16.80	2034.8	695.7
4.0	355.4	15.99	2212.8	747.9	354.7	16.12	2213.0	748.1
4.5	327.7	15.20	2377.1	793.8	326.7	15.37	2377.4	794.1

(assuming zero initial muzzle conditions) are

$$y = \cos\gamma_m \ln(1 + t) + \epsilon \left(\frac{\sin 2\gamma_m}{4}\right) \times \left[\frac{(1+t)^2}{6} + \frac{1}{2} - \frac{2}{3(1+t)} - \ln(1+t)\right] + 0(\epsilon^2) \quad (7a)$$

$$z = \sin\gamma_m \ln(1+t) + \epsilon \left\{\frac{\cos^2\gamma_m}{2}\left[\frac{1}{2} + \ln(1+t) - \frac{(1+t)^2}{2}\right] + \frac{\sin^2\gamma_m}{3}\left[\frac{3}{2} - \frac{1}{(1+t)} - \frac{(1+t)^2}{2}\right]\right\} + 0(\epsilon^2) \quad (7b)$$

In terms of dimensionless quantities, the gravity drop is defined as

$$\Delta z = z(t,0) - z(t,\epsilon) \quad (8)$$

The first-order approximate solution to the gravity drop is obtained from (7b)

$$\Delta z = \epsilon \left\{\frac{\cos^2\gamma_m}{2}\left[\frac{(1+t)^2}{2} - \ln(1+t) - \frac{1}{2}\right] + \frac{\sin^2\gamma_m}{3}\left[\frac{(1+t)^2}{2} + \frac{1}{(1+t)} - \frac{3}{2}\right]\right\} \quad (9)$$

It is noted that solutions to all variables under consideration depend upon the initial flight-path angle. Although the solutions have been expressed as series, the forms are such that comparisons can be made with solutions obtained by alternate methods or those given elsewhere.

For example, employing the Popoff oblique coordinate method[3] to the problem at hand and transforming the results back into rectangular coordinates allow the downrange and altitude variables to be expressed as

$$y = \cos\gamma_m \ln(1+t) \quad (10a)$$

$$z = \sin\gamma_m \ln(1+t) + \frac{\epsilon}{2}\left[\frac{1}{2} + \ln(1+t) - \frac{(1+t)^2}{2}\right] \quad (10b)$$

It is noted that Eq. (10) agree with (7) to first order $0(\epsilon)$ only for the special case of zero initial flight-path angle. Gravity drop obtainable from (10b) does not depend upon initial flight-path angle. In addition, the Popoff method does not allow for gravity coupling to manifest itself into the downrange coordinate for nonzero initial flight-path angles.

Gravity drop given by Ref. 2 in terms of nomenclature employed in this Note is

$$\Delta z = \int_0^t \int \epsilon dt = \frac{\epsilon t^2}{2} \quad (11)$$

For dimensionless time $t < 1$, the terms $\ln(1 + t)$ and $1/(1 + t)$ which appear in (9) can each be expanded as an infinite series. Neglecting terms of higher order than two and substituting the truncated series into (9) allows the resultant to reduce to (11). Thus, the gravity drop as given by Ref. 2 is valid to first order $0(\epsilon)$ only for some small time $t < 1$. Serious errors can occur by using (11) for time $t > 1$.

Gravity drop obtainable from (10b) is somewhat more accurate than that given by (11); however, it is still not formally correct to first order $0(\epsilon)$ except for the special case of zero initial flight-path angle.

Reference 2 also presents a time solution for velocity. The solution expressed in terms of nomenclature employed in this Note is

$$v = 1/(1 + t) \quad (12)$$

Velocity as given by (12) is simply the zeroth-order solution. This is easily seen by taking the parameter ϵ in (6a) as zero. The resultant then reduces to (12).

Numerical Results

A representative light antiaircraft projectile is the Oerlikon 20mm SUL shell.[4] Characteristics of this projectile fired at standard sea level conditions are

$$\bar{v}_m = 1050 \text{ m/sec}, \ \bar{m}\bar{g} = 125.0 \text{ g}, \ \bar{S}_D = 2203 \text{ m}$$

Tables 1–3 list trajectory variables obtained by numerically integrating (1) and (2) and evaluating the first-order approximate solutions as given by (6) and (7) after recasting these equations into dimensional form. The approximate solutions are in excellent agreement with the exact numerical results as can be seen from Tables 1–3.

Conclusions

The basic differential equations governing motion of a light antiaircraft projectile employed against low-altitude targets have been reduced to dimensionless forms. These forms allow approximate solutions to be obtained from an expansion procedure in terms of the small parameter ϵ. The solutions are in excellent agreement with numerical results and can also be used to estimate the order of accuracy of existing solutions. The series solutions converge for any finite time. It should be noted that the solutions do not converge for infinite time because of the appearance of secular terms; however, times of interest are finite. In general, retention of first order $0(\epsilon)$ terms are usually sufficient for analysis purposes.

The approach presented in this note can also be extended to medium caliber antiaircraft projectile ballistics. Medium caliber projectiles are commonly employed against higher-altitude targets. Variation of air density with altitude and variation of drag coefficient with Mach number can be incorporated into the medium caliber projectile solutions in a relatively straightforward manner.

References

[1] Larrabee, E. E., "Aerodynamic Penetration and Radius as Unifying Concepts in Flight Mechanics," *Journal of Aircraft*, Vol. 4, No. 1, Jan.-Feb. 1967, pp. 28–35.

[2] Smith, M. C., "Comments on 'Aerodynamic Penetration and

Radius as Unifying Concepts in Flight Mechanics,'" *Journal of Aircraft*, Vol. 4, No. 4, July-Aug. 1967, pp. 399–400.

[3] McShane, E. J., Kelley, J. L., and Reno, F. V., "Exterior Ballistics," University of Denver Press, Denver, Colo., 1953, Chap. V, pp. 258–283.

[4] "Oerlikon 20mm Belt-Feed Gun, Type 204 GK," Document 2520, 1961, Oerlikon Machine Tool Works, Bührle and Co., Zurich, Switzerland.

Entrance Configuration Effects on Tube Flow in the Transition Regime

JAMES F. MARCHMAN III*
Virginia Polytechnic Institute, Blacksburg, Va.

Nomenclature

C_D = discharge coefficient
D = tube diameter
k = ratio of specific heats
L = total tube length
L/D = tube length-to-diameter
$\dot{m}$ = mass flow rate
P_1 = pressure upstream of the tube entrance
P_2 = pressure downstream of the tube entrance
R = gas constant
Re_D = Reynolds number based on tube diameter
T_1 = upstream temperature
μ_1 = upstream coefficient of viscosity

Introduction

OVER the past seventy years, experimental and theoretical investigations have been conducted on the flow of rarefied gases in tubes and orifices.[1–6] Most theoretical investigations have assumed that the flow entered the tube through an abrupt or square-edged entrance. However, most experimental studies have involved tubes with rounded or bell-mouthed entrances so as to avoid the problem of entrance separation and vena-contracta at higher Reynolds numbers. These experiments have usually specified the tube entrance to be at some point downstream of the rounded entrance in order to compare data with theories assuming fully developed flow at the entrance in the viscous flow range.

In this Note, two recent sets of experimental data[1,4] are compared in order to examine the effect of entrance shape on rarefied flow through tubes and their relation to the theory of Clausing[2] for free molecular tube flow. Clausing's theory depends on the length-to-diameter ratio of the tube, presenting the problem of choosing an effective tube length for a tube with a bell-mouthed entrance.

The recent experimental investigations of Carley and Smetana[1] and Marchman[4] both involved the flow of nitrogen gas through short tubes in the transition regime. Both investigations measured flow rates and upstream and downstream pressures in this range under steady-state conditions and presented data in terms of discharge coefficients,

$$C_D = \dot{m}/[\pi D^2 P_1 (k/R)^{1/2}/4(T_1)^{1/2}]([k+1]/2)^{(k+1)/2(k-1)}$$

and Reynolds number based on tube diameter, $Re_D = 4\dot{m}/\pi D\mu_1$. In both studies flow rates were measured with high accuracy volume displacement flowmeters and pressures with McLeod gages, both of which are calibration standard instruments. All measurements were repeated at least 3 times to insure a high degree of accuracy.

The smooth entrance tube[1] had an entrance-to-exit plane length of 6.22 cm, a constant diameter section downstream

Received April 18, 1969; revision received July 2, 1969.
* Assistant Professor, Department of Aerospace Engineering.

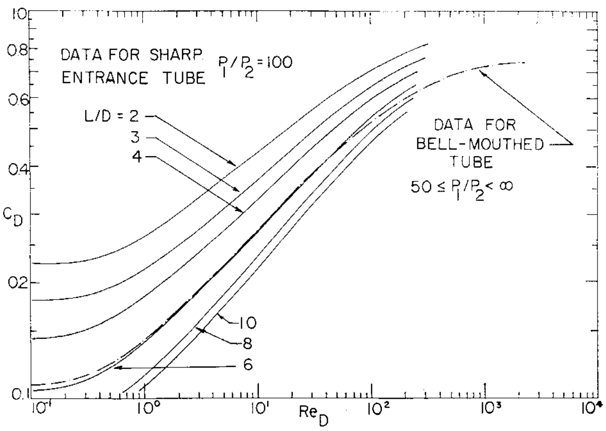

Fig. 1 Comparison of data.

of the entrance of 4.32 cm with a 1.15-cm diam. An effective length-to-diameter ratio of 4.79 was assumed based on an extrapolation of data to the free-molecule limit and comparison with the theory of Clausing. The square-edged entrance tube had a 2.54 cm diam and was tested at L/D values from 2 to 10. The resulting data are presented in Fig. 1. The square-edged tube data are all for pressure ratios of 100 whereas the bell-mouthed tube data are the best curve through the recorded data from pressure ratios of 50 to infinity. A comparison of these curves is valid based on recent studies[1,4,6] which indicate little or no significant increase in discharge coefficient at a given Reynolds number above a pressure ratio of 20. All of the data shown agree with the respective Clausing theory limits for tubes of the given length-to-diameter ratios in the free-molecule limit.

It is noted that at Reynolds numbers from 1 to 30 the bell-mouthed data correspond well with the square-edged data for a length-to-diameter ratio of 6, indicating that the effective length-to-diameter ratio should be nearer to the maximum for this tube (5.42) rather than the value of 4.79 assumed. Below this range of Reynolds number, the rounded entrance tube discharge coefficients exceed those for the square-edge entrance tube, indicating a lower effective L/D. Above this range, the smooth entrance data fall below that for the abrupt entrance indicating a higher effective L/D. While the closeness of the 2 sets of data demands a cautious comparison, a simple analysis of these results would indicate that as the flow approaches free-molecular conditions, the assumption that the rounded entrance can be neglected in computing an effective length becomes more valid. This is indicated by the manner in which the data of Ref. 1 fall remarkably close to those of Ref. 4 for an L/D of 6, while near the free-molecular limit, these data rise above those for the square-edged tube to indicate that the effective L/D of the smooth entrance tube has decreased. At the limit, there is diminishing influence on the flow from molecules reflecting from the wall and hence less retardation of the flow due to the presence of the converging channel. The major influence on the flow is the throat or final tube diameter itself and not the diameter reduction at the entrance. The entrance will always exert some influence on the flow, but as inter-molecular collisions reduce in importance this effect becomes smaller.

In the region above a Reynolds number of 30 the data for the rounded entrance tube again departs from that of the square-edged tube. The indications are that the flow sees an effective tube length even greater than the actual straight tube length. In this range of Reynolds numbers, the viscous forces in the fluid are becoming significant. These viscous effects tend to retard the flow rate in both tubes as is indicated by a decrease in curve slope. However, in the bell-mouth entrance, there is a longer effective wall entrance length actually seen by the flow. This length would be more